Texture attributes for detecting salt bodies in seismic data

Tamir Hegazy and Ghassan AlRegib*
Center for Energy and Geo Processing (CeGP), Georgia Institute of Technology

SUMMARY

Texture-based methods have proven to be useful in the detection of salt bodies in seismic data. In this abstract, we present three computationally inexpensive texture attributes that strongly differentiate salt bodies from other geological formations. The proposed method combines the three texture attributes along with region boundary smoothing for delineating salt boundaries. Our first proposed attribute is *directionality*, which differentiates between regions where texture lacks any specific direction (potentially, salt) and areas with directional texture. The second attribute is the *smoothness* of texture, while the third is based on *edge content*. Our results show that the directionality attribute effectively detects salt bodies in all the seismic images used in testing. The other two attributes correct the false positives detected by the directionality. The overall results show that the proposed method can fairly detect salt regions when compared to manual interpretation.

INTRODUCTION

Interpretation of seismic data involves the recognition of geological structures, including salt bodies. There has been considerable effort in the literature to automate parts of the interpretation process with the goal of improving precision and reduce time. To enable the automation of the interpretation task, texture analysis of seismic data has been proposed by several researchers for salt detection. For example, Berthelot et al. (2013, 2012, 2009) used different texture attributes to detect salt. The texture attributes employed by Berthelot et al. (2009) include the attributes of the gray-level co-occurrence matrix (GLCM), frequency-based attributes, and correlation matrix-based attributes (mean, entropy and smallest eigenvalue). Some of the attributes fail to detect the salt as indicated by Berthelot et al. (2009), while some of them could be computationally complex.

In this paper, we propose texture attributes that are computationally inexpensive, yet highly discriminative against salt regions. Then, we propose a salt region detection method that combines three different texture attributes and then performs boundary smoothing of the delineated area. The first attribute, namely *directionality*, is based on the eccentricity of the scattered plot of the gradient components. Similar to the salt areas, some non-salt regions may also show lack of directionality. Such non-salt regions will be falsely detected as salt by the directionality attribute alone. Therefore, besides directionality, we propose two more correction attributes: *smoothness* and *edge content*. The smoothness attribute helps eliminating regions that are too smooth to be considered part of a salt region, whereas the edge content attribute helps eliminating rough regions that actually belong to edges and not a salt body region.

PROPOSED METHOD

The proposed method has three major components: (*i*) computing texture attributes, (*ii*) combining texture attributes, and (*iii*) smoothing boundaries. In the following subsections, we discuss each component in details.

Texture attributes

In the following, we discuss the three proposed texture attributes. Notably, the proposed three attributes can be used in 2D as well as in 3D seismic volumes. Nevertheless, we limit our experiments in this paper to 2D seismic data sets.

Directionality
As opposed to non-salt regions (e.g., strata), texture in salt regions lacks specific directionality. The directionality attribute captures this fact as follows. For each data point or pixel, we examine the gradient values in a small square window centered around the pixel. We compute the x and the y components of the gradient of intensity values for each pixel in the window. Then, a scattered plot of the x and the y gradient components is generated.

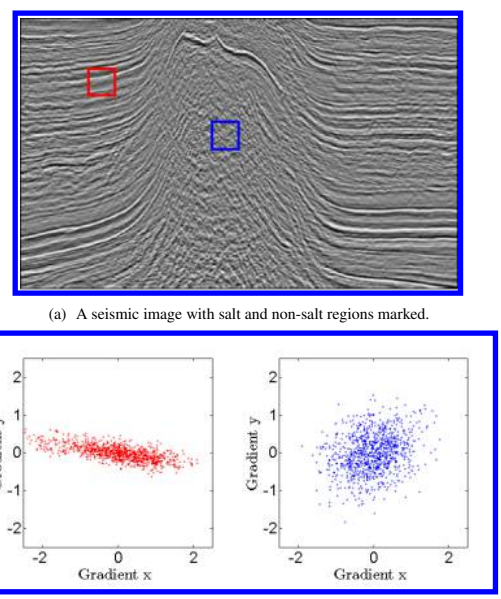

(a) A seismic image with salt and non-salt regions marked.

(b) Scatter plot of gradient components for the marked non-salt region.

(c) Scatter plot of gradient components for the marked salt region.

Figure 1: illustration of the texture directionality attribute within salt and non-salt regions.

Figure 1(a) shows a salt dome in 2D seismic data found in Commissioner (2013). We marked two regions on the image with two squares, such that one of the regions is inside the salt dome, while the other is outside. Figures 1(b) and 1(c) show scattered plots of the gradient for both marked regions. It is

DOI http://dx.doi.org/10.1190/segam2014-1512.1

clear from the plots that the texture of the non-salt region exhibits strong directionality, while that of the salt region lacks it.

Assume that the points of the scatter plot can rotate around a rotation axis that lies in the same plane of the scatter plot. The torque **T** required to generate an angular acceleration **A** is given by:

$$\mathbf{T} = I.\mathbf{A}, \tag{1}$$

where I is the moment of inertia tensor. Since we are considering the case of 2D data at this point, the rotation axis lies in the x-y plane. Therefore, we will drop the z component of the tensor. Further, if the rotation axis is restricted to pass through the centroid $(\bar{x}, \bar{y})$, then it can be shown that:

$$I[x,y] = \sum_{[i,j]\in W_{x,y}} \begin{bmatrix} (G_y[i,j]-\bar{G_y})^2 & (G_x[i,j]-\bar{G_x})(g_y[i,j]-\bar{G_y}) \\ (G_x[i,j]-\bar{G_x})(G_y[i,j]-\bar{G_y}) & (G_x[i,j]-\bar{G_x})^2 \end{bmatrix},$$

where:

- $I[x,y]$ is the moment of inertia tensor for the scattered plot obtained for a neighborhood window $W_{x,y}$ centered around pixel [x,y].
- $W_{x,y}$ is a neighborhood window centered around pixel [x,y]. The summation is performed over all the points in the scatter plot, i.e., for each pixel $[i,j]$ in $W_{x,y}$.
- $G_x[i,j]$ and $G_y[i,j]$ respectively denote the x and y components of the gradient at a given pixel $[i,j]$.
- $\bar{G_x}$ and $\bar{G_y}$ respectively denote the mean of the x and y components of the gradient computed over the neighborhood window $W_{x,y}$.

The eigenvalues of the moment of inertia tensor correspond to the axes of minimum and maximum moments of inertia. Thus, we can use the eigenvalues of the moment of inertia tensor to capture the directionality of texture as follows. Let $\Lambda_1[x,y]$, $\Lambda_2[x,y]$ denote the eigenvalues of $I[x,y]$. We can mathematically define the directionality attribute at pixel [x,y] as:

$$D[x,y] = 1 - \frac{\min(\Lambda_1[x,y], \Lambda_2[x,y])}{\max(\Lambda_1[x,y], \Lambda_2[x,y])}. \tag{2}$$

For non-salt regions, one eigenvalue will be much larger than all other eigenvalues. Thus, the directionality attribute will be close to 1. On the other hand, for salt regions, the eigenvalues will be almost equal, leading to directionality attributes close to zero.

Smoothness

There are cases where the directionality attribute may not differentiate well between salt and some non-salt regions. Figure 2 shows a seismic image with a salt dome found in Sethian (2006). Consider the non-salt region labeled "A" in the figure. The texture of such region does not seem to have strong directionality. Thus, similar to salt regions, the directionality attribute will be close to zero. However, the texture is smoother than that of the salt region. Thus, we introduce the smoothness attribute to complement the directionality attribute in differentiating salt regions. Smoothness is defined as the sum of magnitudes of the gradient over a neighborhood window and can be mathematically formulated as follows:

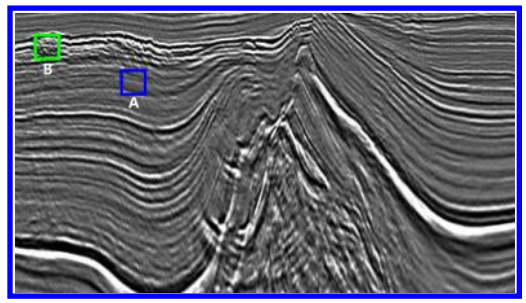

Figure 2: Examples of non-salt regions that can be falsely detected as salt by the directionality attribute.

$$S[x,y] = -\sum_{[i,j]\in W_{x,y}} |G[i,j]|, \tag{3}$$

where $|G[i,j]| = \sqrt{(G_x[i,j])^2 + \left(G_y[i,j]\right)^2}$ is the magnitude of the gradient at pixel $[i,j]$. The negative sign in Eq.(3) ensures that $S[x,y]$ is smaller for non-smooth regions and higher for smooth regions. The gradient computed inside salt regions will have higher magnitudes and hence less smoothness (due to the negative sign) than that of smoother regions.

Edge content

Through our experiments, we came across cases where non-salt regions were confused with salt regions when we used the directionality and the smoothness attributes. Region "B" in Figure 2 is an example. The horizontal directionality is interrupted, causing salt-like appearance. Thus, the directionality attribute, D, is evaluated as a small value. At the same time, the region is not smooth and hence the smoothness attribute, S, is small in value as well. As a result, a false positive will be detected for region "B". However, such regions seem to have an edge-like appearance with stronger variance in gradient values. Although a standard deviation filter over the gradient may capture such edge content, we propose using a range filter to reduce the computational complexity without sacrificing much of the quality. Thus, the edge content attribute can be mathematically defined as:

$$E[x,y] = \max_{[i,j]\in W_{x,y}} |G[i,j]| - \min_{[i,j]\in W_{x,y}} |G[i,j]|. \tag{4}$$

Combining attributes

With the large scale variations within textured regions, the block size to compute the three attributes, $D[x,y]$, $S[x,y]$, and $E[x,y]$ plays an important role. Thus, we compute these attribute values at each pixel a few times given a few different window sizes (5 in our case) and we choose the average of the

DOI http://dx.doi.org/10.1190/segam2014-1512.1

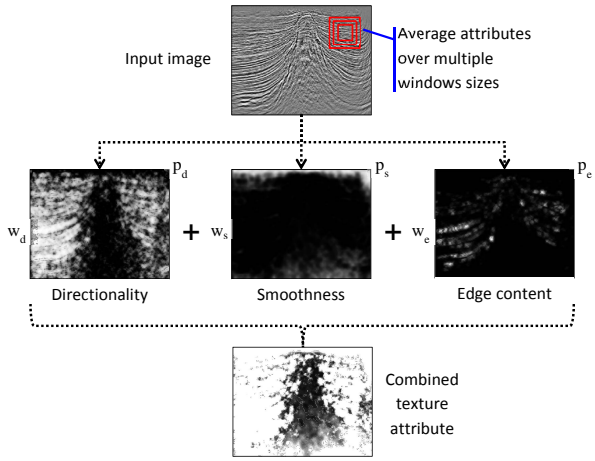

Figure 3: Illustration of the proposed method.

quantities as the attribute value. Typically window sizes range between 5×5 to 50×50 depending on the size of the data set. Further, we linearly scale the attribute values so they range 0 to 1 (inclusive). With $D[x,y]$ already taking values in the range 0 and 1 by definition as shown in Eq.(2), we only need to scale $S[x,y]$ and $E[x,y]$ so that the minimum value is mapped to zero and the maximum value is mapped to 1. We denote the normalized (scaled), averaged attributes as $\hat{D}[x,y]$, $\hat{S}[x,y]$, and $\hat{E}[x,y]$ for directionality, smoothness, and edge content, respectively.

Given the normalized attribute values, the next step is to combine these values into one quantity that could be later thresholded into either a salt dome region or not. In this paper, we use a weighted linear combination of the three quantities. We further apply a non-linear transformation on each attribute value to emphasize large values and de-emphasize small values. This process is illustrated in Figure 3. The overall attribute is given by:

$$A[x,y] = w_d \left(\hat{D}[x,y]\right)^{p_d} + w_s \left(\hat{S}[x,y]\right)^{p_s} + w_e \left(\hat{E}[x,y]\right)^{p_e}, \quad (5)$$

where w's are weights and p's are powers greater than 1.

Smoothing and thresholding

The output of the previous step (Figure 3) is smoothed using a Gaussian filter to remove outliers and isolated points as the ones appear far from the salt dome region in Figure 3. Next, the A map is thresholded. The Gaussian filter parameters and the threshold are set empirically. After thresholding, small regions of the resulting binary image are cleaned up either by morphological operations as suggested by Wallet and Pepper (2013) or by labeling the resulting binary image and keeping the large region(s).

Computational complexity

Let B, N_w, W_{max} denote the seismic image size, the number of different neighborhood window sizes used, and the maximum window size, respectively. The overall worst-case computational complexity for our method is $O(BN_wW_{max})$, i.e., linear complexity in terms of all parameters. This makes our method scalable. The overall worst-case computational complexity can be broken down as follows:

- **Gradient**: Since all of our texture attributes are gradient-based, we compute the gradient as a the first step of our method. A gradient can be computed through one pass over the data set, i.e., in $O(BW_g)$, where W_g is the size of the window used to compute the gradient.
- **Directionality**: Computing the directionality attribute involves computing the moment of inertia tensor, which can be computed in two passes over a neighborhood window. One pass is to compute the centroid (mean), while the other pass is to evaluate the tensor components. As a result the moment of inertia tensor of a single window can be computed in $O(W_{max})$. The subsequent steps of computing eigenvalues and the directionality attribute have complexity of $O(1)$. Since the above operations are repeated for every pixel/voxel in the data set (of size B) and for N_w neighborhood window sizes, then the complexity of computing the directionality map $D[x,y]$ is $O(BN_wW_{max})$.
- **Smoothness and edge content**: Smoothness and edge content attributes are computed by scanning the neighborhood window once for each attribute. Using a similar argument to the one used for directionality, we conclude that their complexity is $O(BN_wW_{max})$.
- **Combining, smoothing and thresholding**: The complexity analysis for these steps is straightforward, and it can be shown that the complexity is $O(B)$, $O(BW_G)$, and $O(B)$, respectively, where W_G is the Gaussian filter window size.

When analyzing the overall complexity, we note that $O(N_wW_{max})$ dominates both $O(W_G)$ and $O(W_g)$. Therefore, the worst-case complexity is $O(BN_wW_{max})$, which means the complexity is actually dominated by the attribute computation (not the subsequent combining/smoothing operations). Yet, it is linear with respect to data size and neighborhood window size, making it attractively scalable.

RESULTS

Figure 4 shows the results of applying the proposed method on four different seismic images that contain salt domes found in Commissioner (2013); Graham (1998); Vinje (2014); Wholefish (2009). Our results (yellow contours in the figure) are compared to manual interpretation (red contours in the figure) conducted by a geophysics doctoral student. In all images, the results are comparable to manual interpretation. In Figure 4(a), our result excludes areas with obvious edge/line contents because of the directionality and edge attributes. Our results also detected and excluded an area with obvious edges that were overlooked by the human interpreter. Note the "hole" close to the bottom of the image. More small regions would have been excluded if we used less aggressive smoothing parameters. In

DOI http://dx.doi.org/10.1190/segam2014-1512.1

Figure 4(b), the main difference between our results and manual interpretation is in the top part of the dome, which was not detected in our case because of the edge on top. The effect of the strong edge was carried through by the neighborhood window and the smoothing filter. The same effect is noticeable to a lesser extent at the top of the dome in Figure 4(c). Finally, in Figure 4(d), the detected salt dome contour fairly tracks the contour defined by the manual interpreter.

CONCLUSIONS AND FUTURE WORK

In this abstract, we introduced three computationally inexpensive texture attributes that can be combined to detect salt bodies in seismic data. The attributes can be applied to the 2D and the 3D cases. The first attribute captures the directionality of the texture. Our experimentation shows that such attribute successfully detects salt in all the data sets we used for testing. However, it occasionally detects false positives. Hence, we defined two more attributes, namely smoothness and edge content, to complement the directionality. Our results show that when the three attributes are combined with the right powers and weights, salt bodies can be detected in a manner close to manual interpretation.

Thus far, the parameters (powers, weights, texture and smoothing window sizes, and Gaussian filter σ) of the method have been adjusted empirically. The main task of our future work is to automatically compute the optimal values of the parameters. Moreover, we are still fine tuning and optimizing our smoothing method. Finally, we seek to compare our method with other automated or semi-automated methods. To that end, we are seeking data sets that other researchers have used in evaluating their methods.

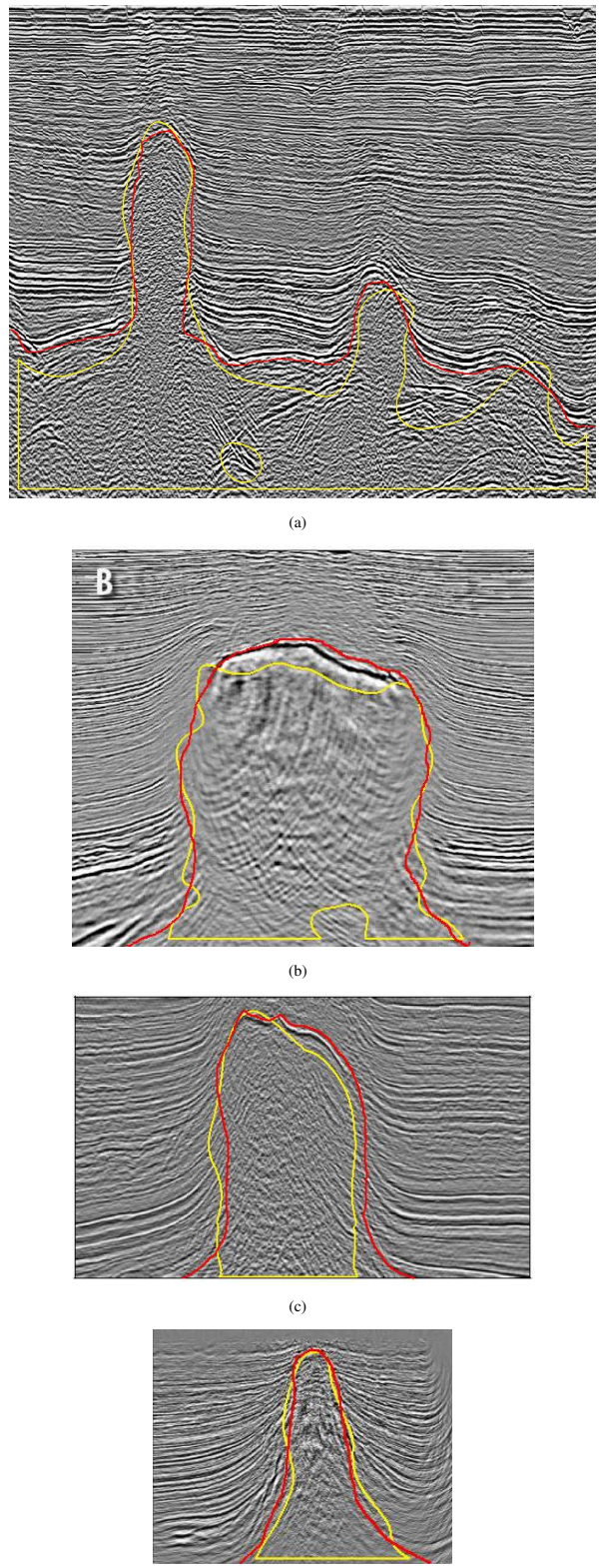

Figure 4: Automatic interpretation results compared with manual interpretation. Yellow contours indicate the results of the proposed method while red contours indicate manual interpretation

DOI http://dx.doi.org/10.1190/segam2014-1512.1

http://dx.doi.org/10.1190/segam2014-1512.1

EDITED REFERENCES

Note: This reference list is a copy-edited version of the reference list submitted by the author. Reference lists for the 2014 SEG Technical Program Expanded Abstracts have been copy edited so that references provided with the online metadata for each paper will achieve a high degree of linking to cited sources that appear on the Web.

REFERENCES

Berthelot, A., A. Solberg, and L. Gelius, 2009, Use of seismic attributes in autotracking of salt structures — A feasibility study: Presented at the Ninth SEGJ International Symposium — Imaging and Interpretation.

Berthelot, A., A. Solberg, and L. Gelius, 2013, Texture attributes for detection of salt: Journal of Applied Geophysics, **88**, 52–69.

Berthelot, A., A. Solberg, E. Morisbak, and L. Gelius, 2012, Use of seismic attributes in auto-tracking of salt structures — A feasibility study: Presented at the 82nd Annual international Meeting, SEG.

Commissioner, G., 2013, Example of a seismic image with salt dome, http://lunar.thegamez.net/coalmining/commissioner-of-geology-and-mining/04062010-detection-of-salt-diapirs-department-of-geosciences-503x314.jpg, accessed on 1 April 2014.

Graham, J., 1998, Example of a seismic image with salt dome, http://astro.berkeley.edu/~jrg/ngst/fft/salt.gif, accessed on 1 April 2014.

Sethian, J., 2006, Example of a seismic image with salt dome, http://math.berkeley.edu/~sethian/2006/Applications/Seismic/seismic_analysis.html, accessed on 1 April 2014.

Vinje, V., 2014, Example of a seismic image with salt dome, http://www.geoexpro.com/articles/2010/04/depth-imaging-seeing-the-invisible , accessed on 1 April 2014.

Wallet, B., and R. Pepper, 2013, Using mathematical morphology in an attribute workflow to improve the interpretability of salt bodies in the Gulf of Mexico: Presented at the 83rd Annual International Meeting, SEG.

Wholefish, 2009, Example of a seismic image with salt dome, http://wholefish.files.wordpress.com/2009/05/salt_domeseismic.jpg, accessed on 1 April 2014.